Uncovering a unique approach for damaged DNA replication: A computational investigation of a mutagenic tobacco-derived thymine lesion

Katie A. Wilson, Carl D. Holland and Stacey D. Wetmore [ID]*

Department of Chemistry and Biochemistry, University of Lethbridge, 4401 University Drive West, Lethbridge, Alberta T1K 3M4, Canada

ABSTRACT

4-(Methylnitrosamino)-1-(3-pyridyl)-1-butanone is a potent nicotine carcinogen that leads to many DNA lesions, the most persistent being the O2-[4-oxo-4-(3-pyridyl)butyl]thymine adduct (POB-T). Although the experimental mutagenic profile for the minor groove POB-T lesion has been previously reported, the findings are puzzling in terms of the human polymerases involved. Specifically, while pol κ typically replicates minor groove adducts, *in vivo* studies indicate pol η replicates POB-T despite being known for processing major groove adducts. Our multiscale modeling approach reveals that the canonical (*anti*) glycosidic orientation of POB-T can fit in the pol κ active site, but only a unique (*syn*) POB-T conformation is accommodated by pol η. These distinct binding orientations rationalize the differential *in vitro* mutagenic spectra based on the preferential stabilization of dGTP and dTTP opposite the lesion for pol κ and η, respectively. Overall, by uncovering the first evidence for the replication of a damaged pyrimidine in the *syn* glycosidic orientation, the current work provides the insight necessary to clarify a discrepancy in the DNA replication literature, expand the biological role of the critical human pol η, and understand the mutational signature in human cancers associated with tobacco exposure.

INTRODUCTION

DNA encodes all information required for human life. However, this information is constantly threatened by many endogenous and exogenous damaging agents (1). Some particularly carcinogenic yet prevalent sources of DNA damage are nicotine products, such as conventional cigarettes and e-cigarette liquid (2,3). The use of tobacco products is associated with several cancers (e.g. lung, head and neck) and it is estimated to account for 30% of cancer deaths worldwide (4). One of the main causes of tobacco-induced cancers is believed to be 4-(methylnitrosamino)-1-(3-pyridyl)-1-butanone (NNK), which is formed *in vivo* when nicotine is metabolized (5–7). In fact, NNK is the only tobacco component that has led to cancer in every species tested (i.e. mice, rats, hamsters, rabbits, pigs, monkeys, and humans) irrespective of the route of exposure (8,9). Within the body, NNK is converted into species that react with DNA to form many different purine and pyrimidine lesions such as methyl (O2-T, O4-T or O6-G), formaldehyde (N6-A, N4-C or N2-G) and pyridyloxobutyl (POB; O2-T, O4-T, N6-A, O6-G, N7-G, O2-C, N3-C or N4-C) adducts (7).

DNA lesions caused by tobacco affect many cellular pathways (10,11). For example, standard DNA replication is typically stalled by damaged nucleobases, and an alternative pathway known as translesion synthesis (TLS) is responsible for replicating past damaged sites. During TLS, at least two polymerases are responsible for replicating damaged sites, with the first polymerase replicating the lesion site and the second polymerase further extending the helix. While this process is critical for preventing cell death, it is error prone and can introduce mutations, which in turn can lead to cancer. Current literature on the replication of DNA adducts arising from known human carcinogens shows that TLS is affected by the chemical structure of the lesion (see, for example, references (12–20)). However, most studies on damaged DNA replication have considered purine lesions (12–18,20,21), while very little is known about the replication of damaged pyrimidines. In fact, only a few damaged pyrimidines have been identified in the literature to date (7,22,23).

A common pyrimidine adduct is O2-[4-oxo-4-(3-pyridyl)butyl]thymine (POB-T; Figure 1A), which is also the most persistent POB adduct formed from NNK, at least in part due to a repair resistance (24,25). Additionally, the mutational signature (signature 4) associated with tobacco smoking in human cancers contains T→A mutations (26) that have yet to be explained, but could be associated with POB-T. As a result, researchers are striving to understand

*To whom correspondence should be addressed. Tel: +1 403 329 2323; Fax: +1 403 329 2057; Email: stacey.wetmore@uleth.ca
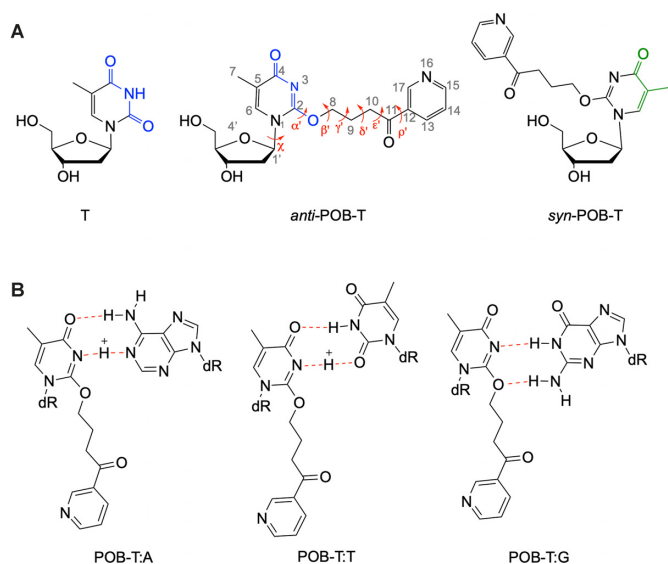
Figure 1. (**A**) The T, *anti*-POB-T and *syn*-POB-T nucleosides, with WC face in blue and Hoogsteen face in green. Key dihedral angles for the lesions include α′ [∠(N1C2O2C8)], β′ [∠(C2O2C8C9)], γ′ [∠(O2C8C9C10)], δ′ [∠(C8C9C10C11)], ε′ [∠(C9C10C11C12)], ρ′ [∠(C10C11C12C13)] and χ [∠(C2N1C1′O4′)]. (**B**) POB-T base pairings previously speculated in the literature (27,28).

the structure and mutagenicity of this T lesion. POB-T is a minor groove lesion (i.e. the bulky moiety is located in the minor groove when the lesion adopts the canonical *anti* orientation about the glycosidic bond) and has an altered Watson-Crick (WC) hydrogen-bonding face compared to canonical T (i.e. N3 becomes a hydrogen-bond acceptor; Figure 1A), and therefore may no longer preferentially pair with A. Indeed, *in vitro* studies indicate that DNA polymerase η (pol η) preferentially inserts dATP and dTTP opposite POB-T, while DNA polymerase κ (pol κ) preferentially inserts dGTP over dATP opposite the lesion (27). Interestingly, the unique outcomes for POB-T replication by pol κ and η indicate that these two human TLS polymerases process the lesion in different ways, although the exact pathways are currently unknown.

To clarify the polymerase responsible for POB-T bypass *in vivo*, single and double knockdown or knockout strains of human cells (HEK293K) were constructed for pol η, κ, ι and ζ, and Rev1 (28,29). These strains show that pol η and ζ have a significant effect on lesion bypass (bypass efficacy reduced from < 55% in wild-type cells to < 36% in the mutant cells), while knockdown or knockout of pol κ, ι or Rev1 did not substantially change the efficiency of TLS past POB-T (28,29). The results from knockdown and knockout strains are consistent with *in vitro* work indicating that pol η most efficiently bypasses POB-T (27). Nevertheless, pol η replicates POB-T ~1000-fold less efficiently than natural DNA (27). Furthermore, in wild-type cells, T→A mutations (i.e. dTTP incorporations) occur at a high frequency (up to ~50%) regardless of the organism (i.e. *Escherichia coli*, mice, or humans) (28–32). These *in vivo* studies are consistent with POB-T replication by pol η, since *in vitro* stud-

ies indicate that pol η most commonly inserts dTTP opposite POB-T (27). However, these conclusions contrast literature suggesting pol κ replicates minor groove lesions (33), while pol η replicates pyrimidine dimers and major groove adducts (34–37). Indeed, pol κ has an open pocket on the minor groove side of the DNA duplex that can accommodate a bulky moiety, while pol η has an open pocket that aligns with the DNA major groove (38,39). Nevertheless, pol κ has been proposed to require WC hydrogen bonding for rapid catalysis (28,40), a condition that is not satisfied by POB-T.

There is currently no structural information available for POB-T replication. However, hydrogen-bonding patterns between the lesion and the canonical nucleobases have been proposed to rationalize the observed lesion mutagenicity. Specifically, the prevalence of dGTP insertion by pol κ was speculated to arise due to the formation of two hydrogen bonds between POB-T and dGTP (Figure 1B) (27,41). On the other hand, the observed insertion of dATP and dTTP by pol η (27,41) was explained based on interbase hydrogen bonding involving protonation of the lesion (i.e. at N3) or the pairing base (i.e. at N1 of A or O2 of T) (Figure 1B) (27,28). However, the authors acknowledge that these proposed pairs do not explain why dGTP is not inserted by pol η (27,41). Additionally, mass spectrometry data indicates that POB-T is not cationic (42), and there is no evidence to support the protonation of the canonical DNA nucleobase interacting with POB-T. It has therefore been suggested that protein–DNA interactions may play a large role in dictating dNTP insertion opposite POB-T (27,28). Thus, detailed structural information about the lesion and polymerase-DNA complex is required to elucidate factors that control POB-T replication by pol κ and η.

Previous work on other DNA lesions has shown that computational chemistry is an important tool for gaining molecular level insight into the function of DNA polymerases, including lesion accommodation within the active site and mutagenic outcomes (see, for example, references (33,43–50)). Therefore, the present work uses density functional theory (DFT) calculations and molecular dynamics (MD) simulations to provide the first structural information for POB-T, as well as the preferred base pairings and lesion replication. Specifically, DFT nucleobase models reveal the intrinsic conformational preference about the nucleobase–bulky moiety linker and within the bulky moiety of POB-T. Next, docking and MD simulations uncover how the lesion is accommodated in the pol κ and η active sites prior to dNTP binding. DFT models of isolated hydrogen-bonded pairs provide insight into possible interactions between POB-T and the canonical nucleobases. Finally, MD simulations on insertion complexes shed light on how pol κ and η replicate POB-T and rationalize the varying propensities for dNTP insertion. Overall, our multiscale computational approach provides the structural insight necessary to clarify the apparent discrepancy in the DNA replication literature by highlighting differences in how two critical human TLS polymerases replicate POB-T and thereby expands the biological role of pol η.

MATERIALS AND METHODS

DFT calculations

Barriers about key rotatable bonds in the POB-T nucleobase (α', β', γ', δ', ϵ' and ρ', Figure 1A) were determined using B3LYP-D3(BJ)/6–31G(d). To gain a more complete picture of possible POB-T nucleobase orientations, an AMBER99 conformational search with respect to the same geometrical features was performed as implemented in HyperChem. All resulting lesion orientations were subsequently optimized using B3LYP-D3(BJ)/6–31G(d) and the relative energies determined using B3LYP-D3(BJ)/6–311++G(2df,2p). Hydrogen-bonded dimers between the WC or Hoogsteen face of POB-T and the canonical nucleobases were investigated using B3LYP-D3(BJ)/6–311++G(2df,2p)//M06–2X/6–31G(d). Reported binding energies include zero-point vibrational energy corrections, but do not include basis set superposition error corrections or monomer deformation energies. All calculations were performed using Gaussian 09 (revision D.01).

MD simulations

The orientation of POB-T in the pol κ and η active sites was initially investigated by overlaying the nucleobase conformations (adducted T heavy atoms) identified in the conformational search onto the template T in a pol κ or η crystal structure (PDB IDs: 5W2C and 4ECS) corresponding to dATP insertion. Representative lesion orientations were then used to initiate MD simulations (AMBER ff14SB) on the pol κ and η preinsertion and insertion complexes with select dNTPs.

All complexes were solvated in a TIP3P octahedral water box such that the solute was at least 10.0 Å from the box edge. NaCl was added to DNA–polymerase systems to yield an $\sim$0.150 M concentration. Mg^{2+} ions were included in the insertion complexes. While we recognize that this does not represent the native environment of the enzyme in a cell, this is the conventional approach used in the literature to understand the structure of polymerase complexes (see for example, references (33,43–50)). All systems were minimized, heated to 310 K, and equilibrated. Multiple 20 ns unconstrained pre-production simulations were performed to identify geometries that were distinctly different from the initial structures and cannot be easily converted during standard MD sampling. Structures of the polymerase–DNA complexes with a hydrogen-bonding geometry and lesion orientation most conducive for the reaction were selected as initial structures for subsequent pre-production 100 ns MD simulations, which were run in triplicate to ensure statistical significance. Since the replicas lead to minimal differences in the active site region (rmsd of 0.7–1.8 Å), one replica was extended to yield the final 0.5 µs MD production simulation results discussed in the main text. While analysis was performed on the entire trajectory (frames spaced by 0.1 ns), a representative structure was chosen for figures based on the lesion orientation and hydrogen bonding. Furthermore, the strengths of interactions between the dNTP and lesion were estimate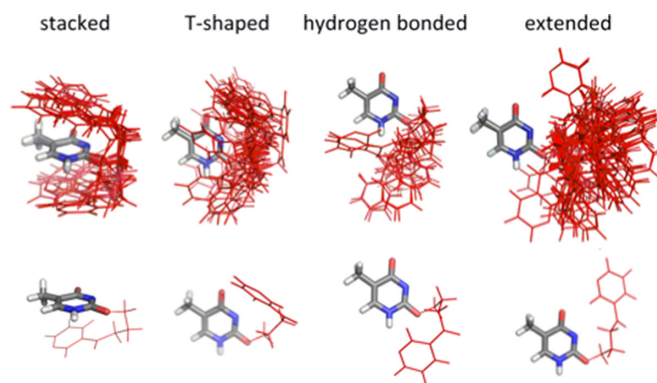d using gas-phase B3LYP-D3(BJ)/6–311++G(d,p) energies on isolated hydrogen-capped nucleobase dimers. All MD simulations were performed using AMBER 14.

Full details of the computational protocol are provided in the Supplementary Information.

Figure 2. Overlay of DFT POB-T nucleobase conformations (based on damaged T heavy atoms, bulky moiety highlighted in red, top) and most stable conformer from each category (bottom).

RESULTS AND DISCUSSION

POB-T is a highly flexible lesion

DFT was used to understand the inherent structural preference about the nucleobase–carcinogen linker and within the bulky moiety. Calculations initiated from a linear orientation (i.e. α', β', γ', δ', ϵ' and $\rho' = 180°$, Figure 1A) indicate that the bulky moiety exhibits a $\sim$41 kJ/mol preference to be positioned toward the WC face at the nucleobase–carcinogen linker (i.e. first carbon of the bulky moiety directed toward N3), with the corresponding rotational barrier being $\sim$45 kJ/mol (Supplementary Figures S1 and S2). Nevertheless, POB-T is highly flexible about all other key bulky moiety dihedral angles (minima within $\sim$5.5 kJ/mol and rotational barriers of <30 kJ/mol; Supplementary Figures S1 and S2). Therefore, the interplay between various bulky moiety orientations needs to be considered.

Since understanding the inherent structural preference of POB-T using isolated rotational barriers neglects the interplay between various rotatable bonds, a conformational search was performed to gain insight into the minimum energy orientations of the lesion. The resulting 164 unique adduct conformations (Supplementary Figure S3) were visually inspected and classified based on the interactions between the bulky moiety and the adducted T as stacked, T-shaped, hydrogen bonded or extended (no interaction; Figure 2). Although there is substantial structural and energetic (up to $\sim$50 kJ/mol) variation within each conformational category (Figure 2 and Supplementary Figure S4), the majority of accessible POB-T conformations are extended (49%), while there is an approximately equal number of stacked and T-shaped structures ($\sim$20% each), and fewer hydrogen bonded conformers (10%; Supplementary Figure S4A). However, many of the hydrogen bonded, T-shaped and extended conformations will not fit within the confines of the DNA helix due to the close proximity of the bulky moiety and the site of backbone attachment (Figure 2). Re-
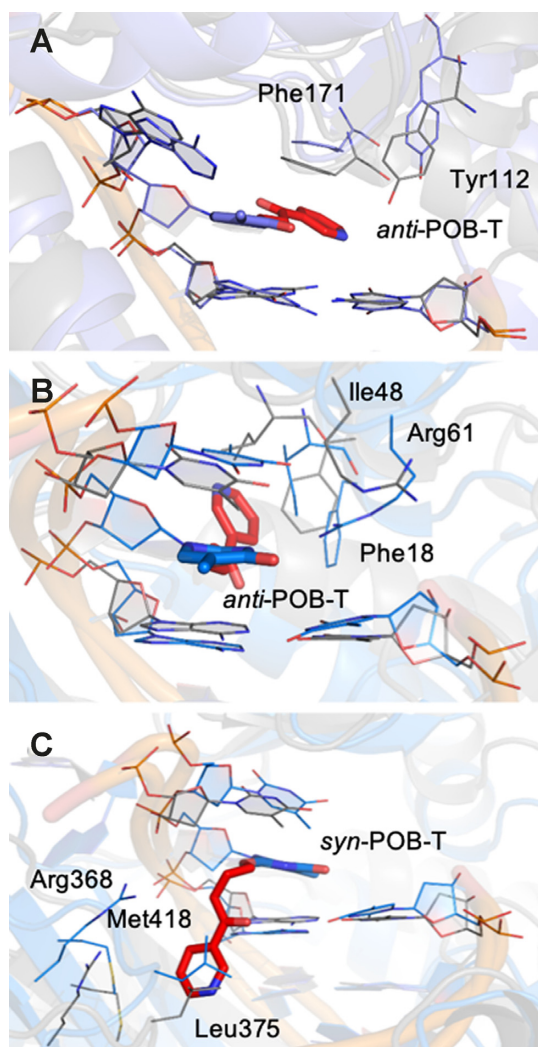
Figure 3. Overlay of MD representative structures for (**A**) *anti*-POB-T bound in the pol κ active site (purple) and (**B**) *anti*-POB-T or (**C**) *syn*-POB-T bound in the pol η active site (blue) with crystal structures (grey) for dATP insertion opposite dT (PDB ID: 5W2C for pol κ and 4ECS for pol η).

gardless, the lesion displays a consistent orientation at the nucleobase–carcinogen linker (i.e. first carbon of the bulky moiety is directed toward the WC face) and the bulky moiety is rarely linear in the 52 lowest energy structures (relative energy < 20 kJ/mol; Supplementary Figure S5).

POB-T can adopt the canonical *anti* glycosidic orientation in the pol κ active site, while only *syn*-POB-T can be accommodated by pol η

The orientation of POB-T in the pol κ and η active sites prior to dNTP insertion was investigated to gain insight into the impact of the enzyme and surrounding DNA on the lesion conformation. Initially, all POB-T conformers identified in the conformational search were manually docked into the pol κ active site such that the lesion adopts the canonical *anti* conformation about the glycosidic bond. Although most conformations of the isolated POB-T nucle-
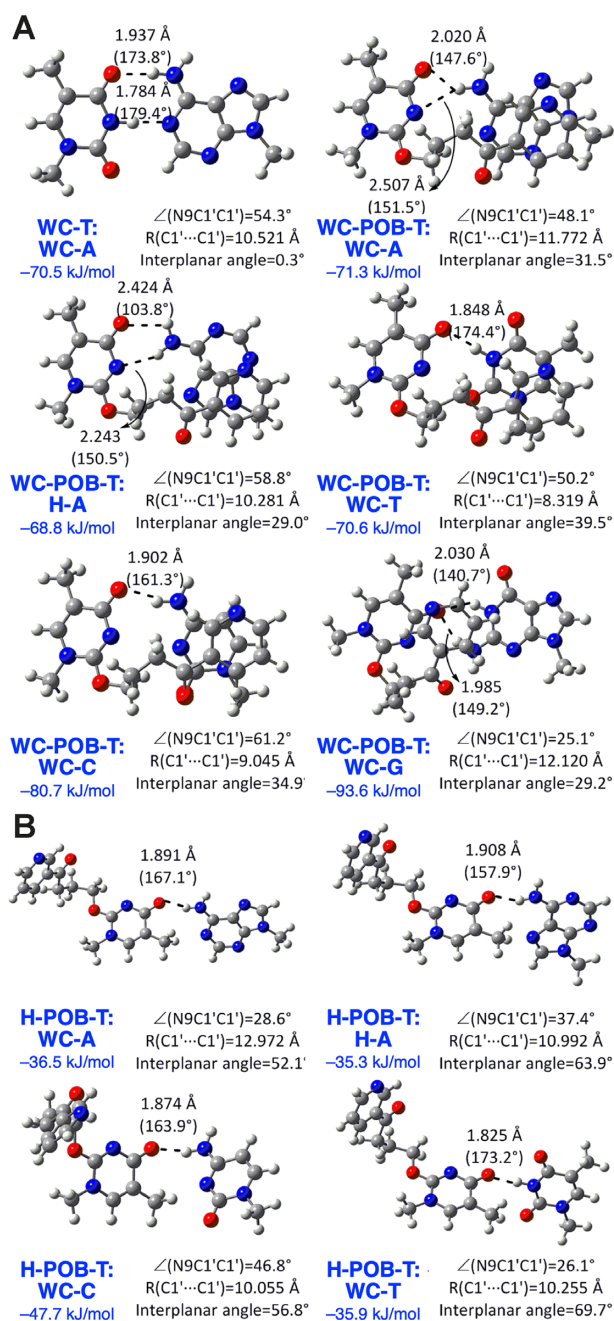

Figure 4. DFT structures and binding energies for base pairs between the (**A**) T or POB-T WC face or (**B**) POB-T Hoogsteen (H) face and the canonical nucleobases.

obase do not fit in the pol κ active site, 37 of the 164 conformations are well accommodated (closest heavy atom distance between the lesion and polymerase or DNA > 2.0 Å; Supplementary Figure S6). All 37 conformers adopt an extended orientation, the most common conformation of the isolated nucleobase. When MD simulations (0.5 μs) were performed on the pol κ preinsertion complex, POB-T adopts orientations that span all 37 manually docked conformations (Supplementary Figure S7). These orientations position the bulky moiety in an open pocket near the little finger domain and away from the dNTP binding site of pol
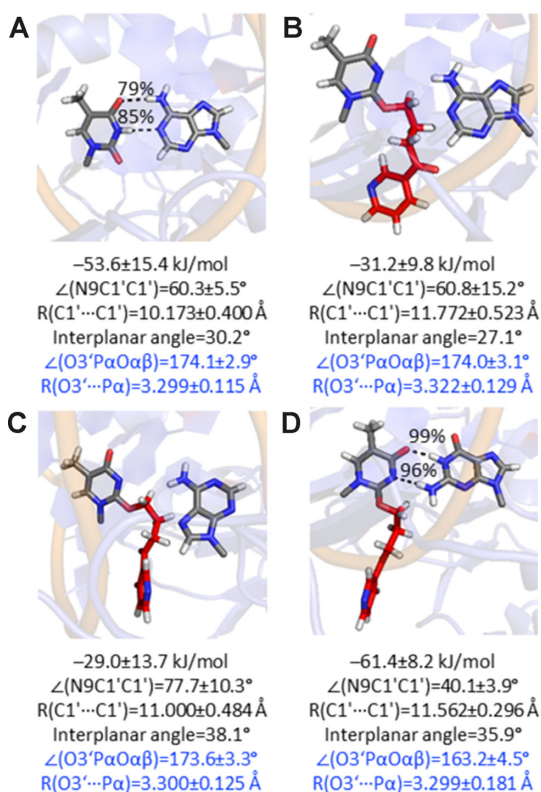
Figure 5. Structure and reaction coordinates for pol κ insertion of dATP opposite (**A**) T or (**B**) POB-T, and (**C**) *syn*-dATP or (**D**) dGTP insertion opposite POB-T.
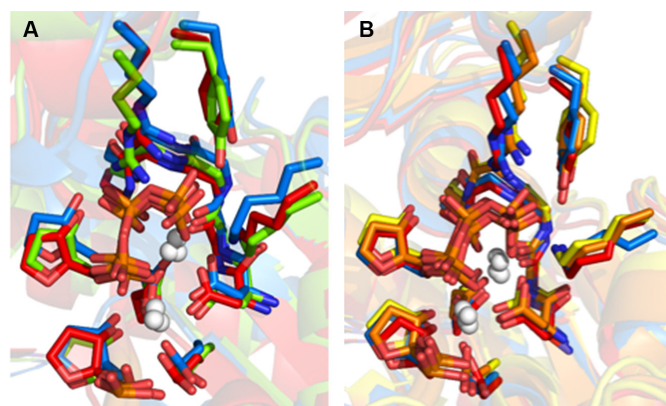

Figure 6. Overlay (based on polymerase backbone) of *anti*-dATP (blue), *syn*-dATP (red), dCTP (yellow), and dGTP (green) insertion complexes for POB-T replication by (**A**) pol κ or (**B**) pol η.

Figure 7. Structure and reaction coordinates for pol η insertion of dATP opposite (**A**) T or (**B**) POB-T, and (**C**) *syn*-dATP, (**D**) dCTP or (**E**) dTTP insertion opposite POB-T.

κ. There is little change in the overall polymerase structure upon POB-T accommodation compared to a crystal structure of T replication (rmsd $= 1.244 \pm 0.206$ Å for the active site region; Figure 3A). This accommodation of POB-T correlates with evidence that pol κ replicates minor groove adducts, such as N2-G and N3-A lesions (38,39).

Since pol η is generally believed to replicate major groove lesions (51), it is not clear how the enzyme exerts activity towards the minor groove POB-T adduct. Indeed, when all POB-T nucleobase orientations were manually docked into
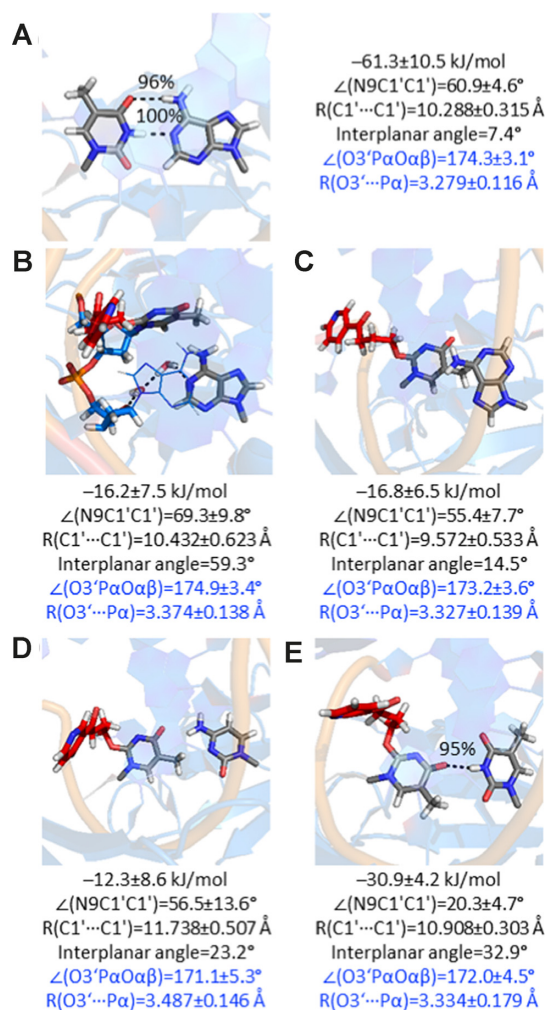
the pol η active site using the same protocol applied to pol κ, only 8 of the 164 conformations fit in the pol η active site (Supplementary Figure S8). However, these eight conformations correspond to extended orientations that place the bulky moiety in close proximity to key residues in the catalytic palm domain (e.g. Phe18 and Arg61) and/or the binding position of the incoming dNTP. When MD simulations (0.5 μs) were performed on this complex, POB-T adopts orientations that span all 8 manually docked conformations (Supplementary Figure S9). Furthermore, MD simulations reveal disruptions in the active site region compared to the X-ray crystal structure, in particular changes in the positions of Phe18 (rmsd $= 1.883 \pm 0.512$ Å), Ile48 (rmsd $= 2.221 \pm 0.436$ Å) and Arg61 (rmsd $= 2.513 \pm 0.923$ Å), which will compromise dNTP binding (Figure 3B). Notably, Phe18 stacks with the POB-T pyridyl ring, leading to a Phe18 orientation that would prevent dNTP binding. Furthermore, there is no space within the pol η active site to accommodate movement of the bulky moiety and therefore Phe18, to permit dNTP binding without introducing steric clashes. Thus, the predicted disrupted pol η active site con-

formation upon accommodation of POB-T is irreversible. This suggests that *anti*-POB-T is not bypassed by pol η, which is consistent with the lack of replication of other minor groove lesions by pol η (38,39), but contradicts *in vivo* and *in vitro* studies on POB-T (27,28,41). Nevertheless, pol η may accommodate POB-T in a different conformation.

A change in the glycosidic conformation for POB-T was considered as the addition of various bulky moieties to purine nucleosides induces a *syn* glycosidic conformation (14,52,53). Although no such preference has been previously reported for a pyrimidine lesion, our DFT calculations suggest that the *syn*-POB-T conformation is only ∼9 kJ/mol higher in energy than the *anti* conformation and the two conformations are connected by a modest ∼35 kJ/mol barrier (Supplementary Figure S10). When *syn*-POB-T was manually docked into the pol η active site, significantly more POB-T conformations can be accommodated by pol η compared to *anti*-POB-T (30 versus 8; Supplementary Figure S8 and S7). These conformations extend the bulky moiety on the major groove side of the growing helix and into an open pocket near the pol η little finger domain. Subsequent MD simulations reveal the POB-T bulky moiety adopts many conformations with respect to the adducted T. Nevertheless, changes in the little finger domain, in particular disruptions in Arg368 (rmsd = 4.545 ± 0.610 Å), Met418 (rmsd = 4.557 ± 0.425 Å) and Leu375 (rmsd = 5.479 ± 0.733 Å), occur to accommodate the lesion (Figure 3). These changes will likely have a much smaller impact on dNTP insertion than the disruption of the catalytic palm domain seen for *anti*-POB-T. In fact, when POB-T is bound in the pol η active site in the *syn* orientation, there is space for an incoming dNTP to bind. While damaged purines have been shown to adopt a *syn* glycosidic orientation during replication (14,52,53), to the best of our knowledge this is the first evidence suggesting that a pyrimidine adopts the *syn* glycosidic conformation within a polymerase active site. Nevertheless, other nucleic processing enzymes, such as the TET family of enzymes (54), the NEIL1 DNA repair enzyme (55), and functional RNA (56), bind pyrimidines in the *syn* conformation. The unique POB-T glycosidic orientations accommodated by pol κ and η may explain the observed differential replication outcomes, which will be probed in the following sections by analyzing the corresponding dNTP insertion complexes.

Pol κ adopts a catalytically conducive conformation for the insertion of dGTP opposite POB-T

Prior to investigating the POB-T base-pairing preferences in the pol κ active site, DFT calculations were used to explore potential hydrogen bonding between the POB-T WC face and each canonical nucleobase (Figure 4). POB-T was considered in the extended conformation, the only orientation accommodated by pol κ. In all dimers, a stacking interaction occurs between the POB-T bulky moiety and the pairing base, which complements interbase hydrogen bonding to stabilize the base pairs (Figure 4A). When POB-T is paired with A or G, two hydrogen bonds occur (Figure 4A). Nevertheless, POB-T pairing with G (∼−94 kJ/mol) is significantly stronger than with A (∼−70 kJ/mol). Furthermore, the POB-T:G hydrogen-bonding geometry is different from that proposed in the literature (27,28) (Figure 1B) since our predicted orientation at the carcinogen–nucleobase linker directs the first carbon of the bulky moiety toward the lesion WC face and thus prevents O2 of the lesion from hydrogen bonding with the pairing G. Finally, POB-T mispairs with T or C contain a single hydrogen bond and have interaction energies of −70.6 or −80.7 kJ/mol, respectively (Figure 4A). All POB-T pairs are non-planar (interplanar angle ≈ 30°). Additionally, the base pairs exhibit distortion in the canonical base pair width (by up to 2.2 Å) and/or opening (by up to 30°), with the exception of the POB-T:*syn*-dATP pair, which maintains a width and opening consistent with canonical DNA.

To gain a better understanding of POB-T replication by pol κ, MD simulations on the pol κ insertion complexes with dGTP or dATP paired opposite POB-T were performed. These pairs were considered since G and A form two hydrogen bonds with POB-T in the isolated base pairs and these pairs are observed experimentally (27,41). Conversely, pairing C and T lead to only a single hydrogen bond with POB-T and do not correlate with an experimentally-observed mutagenic outcome, and thus these pairs were not considered in the polymerase active site. Regardless of the opposing base, the bulky moiety adopts many distinct extended conformations in the insertion complexes. Nevertheless, the first carbon of the bulky moiety is preferentially directed toward the lesion WC face as observed for the isolated nucleobase (Supplementary Figure S11). The bound POB-T orientation consistently positions the bulky moiety in an open pocket of pol κ, where a hydrogen bond occurs between the bulky moiety N and Ser102 (Supplementary Tables S1–S3). The steric constraints of the active site prevent interactions between the bulky moiety and opposing base, which will destabilize the pairs. This contrasts the isolated base pairs in which the bulky moiety interacts with the opposing base.

To correctly align the dNTP for the phosphoryl transfer reaction, a number of active site features must be maintained, including octahedral coordination of the catalytic and binding Mg^{2+} ions, a reaction distance [d(3′-primer end(O3′)–dNTP(Pα)] of < 3.5 Å and a reaction angle [∠(3′-primer end(O3′)–dNTP(Pα)–dNTP(Oαβ))] of ∼180° (57–59). These criteria are satisfied for dATP and dGTP insertion opposite POB-T by pol κ (Figure 5 and Supplementary Table S4). In addition, minimal differences occur in the interactions between the dNTP backbone, and the surrounding amino acids compared to dATP insertion opposite T (Figure 6A and Supplementary Tables S1-S3 and S5).

Despite the correct alignment of the reaction coordinate, the largest differences in the dATP and dGTP pol κ insertion complexes occur in the nascent base pair. Specifically, POB-T does not hydrogen bond with an incoming dATP (Figure 5). Instead, the bulky moiety chain or pyridyl ring forms non-covalent C–H···π and π···π interactions with dATP (Supplementary Figure S11). This leads to an average POB-T:dATP interaction energy of ∼−30 kJ/mol. Therefore, despite the reaction coordinate being aligned for catalysis, weak interactions occur between POB-T and dATP. Overall, this correlates with *in vitro* kinetic data suggesting that dATP is infrequently inserted opposite POB-T by pol κ (27,41).

Although POB-T:dGTP is distorted compared to undamaged DNA (deviations in base pair width of ∼1 Å and opening of ∼20°), the POB-T(O4)···dGTP(N1H) and POB-T(N3)···dGTP(N2H) hydrogen bonds are persistent (>95%; Figure 5D). This leads to an average interaction strength of –61.4 kJ/mol, which is ∼13 or ∼30 kJ/mol stronger than canonical T:dATP or POB-T:dATP, respectively (Figure 5D). When coupled with the catalytic orientation of the reaction coordinate, this correlates with experimental *in vitro* kinetic studies that indicate dGTP is inserted opposite POB-T at a higher rate than dATP (27). Although our calculations rationalize the *in vitro* data, *in vivo* studies indicate that knockout of pol κ does not influence POB-T replication and therefore it is unlikely that pol κ replicates POB-T *in vivo* (28). Since the predicted insertion complexes are aligned for catalysis, our data supports suggestions that the decreased reactivity of pol κ towards POB-T may stem from the lack of WC hydrogen bonding, which is proposed to be required for rapid catalysis (28,40).

Unique *syn* glycosidic orientation explains experimentally observed dTTP and dATP insertion opposite POB-T by pol η

MD simulations on preinsertion complexes predict that an extended orientation of POB-T is accommodated in the pol η active site in the *syn,* but not the canonical *anti,* glycosidic orientation. However, it is unclear how the POB-T Hoogsteen face interacts with the canonical nucleobases. DFT calculations on pairs between the POB-T Hoogsteen face and the canonical nucleobases reveal no interactions between the bulky moiety and any canonical pairing base. Although a stable Hoogsteen-POB-T:G base pair could not be isolated, a single hydrogen bond occurs between POB-T(O4) and A(N6H), C(N4H), or T(N3H) (Figure 4B). As a result, pairs involving the POB-T Hoogsteen face are all significantly less stable than canonical T:A (by 22 – 35 kJ/mol) and pairs involving the POB-T WC face (by 21–59 kJ/mol). Additionally, while all *syn*-POB-T base pairs retain the width of canonical DNA, the pairs are significantly nonplanar (by up to ∼70°) and distorted with respect to the opening (by up to ∼30°). The consistent weak and distorted interactions between the POB-T Hoogsteen face and the canonical nucleobases correlate with reports that pol η has a low dNTP selectivity during POB-T replication (27,41).

To further understand the POB-T replication outcomes MD simulations on the pol η insertion complexes were performed. Specifically, dATP, dCTP, and dTTP were paired opposite the lesion in the pol η active site, since A, C and T all form a hydrogen bond with POB-T in the nucleobase pairs. In all complexes, there is substantial variation in the bulky moiety conformation (Supplementary Figure S12). However, the lesion preferentially adopts an extended orientation that directs the bulky moiety away from the pairing base, toward the previously replicated DNA, and near residues in the little finger domain (i.e. Arg368, Met418, and Leu375). Additionally, as observed for pol κ, all pol η insertion complexes maintain octahedral coordination of the catalytic and binding Mg^{2+} ions (Supplementary Table S4), and the reaction distance and angle are < 3.5 Å and 170–175°, respectively (Figure 7). Furthermore, regardless of the pairing base, interactions between the dNTP backbone and surrounding amino acids are similar to those for the replication of T (Figure 6B and Supplementary Tables S6–S10). Therefore, all complexes contain a catalytically conducive active site orientation.

Despite a consistent N–H···POB-T(O4) hydrogen bond with A, C or T in the lesion nucleobase pairs, differences occur in the interactions between the dNTP and *syn*-POB-T in the pol η active site. Indeed, steric constraints within the active site force *syn*-POB-T:*syn*-dATP and *syn*-POB-T:dCTP into geometries that lack interbase hydrogen bonding (Figure 7). This suggests that neither *syn*-dATP nor dCTP will be selectively incorporated opposite the lesion by pol η. Interestingly, when dATP is placed opposite *syn*-POB-T, the lesion flips out of the helix into the major groove and toward the little finger domain of pol η. With *syn*-POB-T out of the helix, dATP is stabilized in the active site by a water-bridged hydrogen bond between dATP(N1) and the 3′-A(O4′) (Figure 7 and Supplementary Figure S13B). This is similar to the reported replication of one of the most common types of DNA damage, namely an abasic site. Specifically, a crystal structure of dATP insertion opposite an abasic site by pol η shows a water-bridged hydrogen bond between the dATP nucleobase and the template backbone (60). This indicates that the experimentally-observed insertion of dATP opposite POB-T (27,28,41) likely occurs in a manner analogous to the replication of an abasic site.

In contrast to dCTP and dATP, dTTP paired opposite *syn*-POB-T by pol η leads to the POB-T(O4)···dTTP(N3H) (95%) hydrogen bond (Figure 7E), which contribute to an average interaction energy of –30.9 kJ/mol. Nevertheless, while the pair maintains a width consistent with natural DNA, it is not planar (interplanar angle = 33°). Since T is the only nucleobase that can directly interact with POB-T in the pol η active site, our simulations provide the first structural explanation for *in vitro* studies that indicate pol η preferentially inserts dTTP opposite POB-T (27,41), as well as *in vivo* studies that report POB-T leads to T→A mutations (28). Our new proposal that pol η bypasses POB-T in the *syn* glycosidic conformation sheds light on the differential POB-T replication outcomes for pol κ and η, and to the best of our knowledge provides the first evidence that a polymerase can replicate a damaged *syn* pyrimidine.

CONCLUSION

Our multiscale modeling provides the first structural information on the minor groove POB-T lesion, and thereby rationalizes the previously confusing mutational spectrum (27,28,41). Indeed, although pol κ typically replicates minor groove lesions, pol κ has been reported to insert dGTP opposite POB-T *in vitro,* but does not replicate the lesion *in vivo* (27,28,41). In contrast, *in vivo* work indicates that POB-T is replicated by pol η, which typically bypasses major groove lesions, and this replication leads to up to ∼ 50% T→A mutations (27,28,41). Our results further clarify the role of these human polymerases by predicting that POB-T adopts different glycosidic orientations in the pol κ and η active sites. Specifically, *anti*-POB-T can fit in the pol κ active site and this orientation preferentially pairs with dGTP, which correlates with the experimentally observed replica-

tion outcome (27,28,41). Conversely, *anti*-POB-T cannot be accommodated by pol η and instead the *syn* conformation is adopted. In the *syn* conformation, the lesion preferentially pairs with dTTP, which correlates with previous reported *in vitro* and *in vivo* pol η data (27,28,41). We propose that the experimentally-observed non-mutagenic replication of POB-T by pol η occurs through stabilization of dATP opposite POB-T in a manner analogous to dATP insertion opposite a common type of DNA damage, namely an abasic site (60), rather than through conventional WC hydrogen bonding. All lesion conformations and associated hydrogen-bonding patterns between POB-T and the canonical nucleobases calculated in the present work differ from those previously hypothesized in the literature in the absence of accurate structural data, thus highlighting the need for this fundamental information. Nevertheless, future work is required to clarify the structural basis of extension past the lesion site. Overall, the current work provides the structural insights necessary to clarify an apparent discrepancy in the DNA replication literature by expanding the biological role of pol η. Furthermore, although other nucleic acid binding enzymes have been shown to bind pyrimidines in the *syn* glycosidic conformation (54–56), our results provide the first evidence for the replication of a *syn* pyrimidine. Most importantly, the current work provides structural support that indicates POB-T may lead to the T→A mutations observed the mutational signature (signature 4) associated with tobacco smoking in human cancers (26).

SUPPLEMENTARY DATA

Supplementary Data are available at NAR Online.

ACKNOWLEDGEMENTS

FUNDING

REFERENCES

1. De Bont,R. and van Larebeke,N. (2004) Endogenous DNA damage in humans: A review of quantitative data. *Mutagenesis*, **19**, 169–185.
2. Bilano,V., Gilmour,S., Moffiet,T., D'Espaignet,E.T., Stevens,G.A., Commar,A., Tuyl,F., Hudson,I. and Shibuya,K. (2015) Global trends and projections for tobacco use, 1990–2025: An analysis of smoking indicators from the WHO comprehensive information systems for tobacco control. *Lancet.*, **385**, 966–976.
3. Harris,C.C. (2018) Tobacco smoking, e-cigarettes, and nicotine harm. *Proc. Natl. Acad. Sci. U.S.A.*, **115**, 1406–1407.
4. Hang,B. (2010) Formation and repair of tobacco carcinogen-derived bulky DNA adducts. *J. Nucleic Acids*, **2010**, 29.
5. Hecht,S.S. (2003) Tobacco carcinogens, their biomarkers and tobacco-induced cancer. *Nat. Rev. Cancer*, **3**, 733.
6. Lee,H.W., Park,S.H., Weng,M.W., Wang,H.T., Huang,W.C., Lepor,H., Wu,X.R., Chen,L.C. and Tang,M.S. (2018) E-cigarette smoke damages DNA and reduces repair activity in mouse lung, heart, and bladder as well as in human lung and bladder cells. *Proc. Natl. Acad. Sci. U.S.A.*, **115**, E1560–E1569.
7. Peterson,L.A. (2016) Context matters: Contribution of specific DNA adducts to the genotoxic properties of the tobacco-specific nitrosamine NNK. *Chem. Res. Toxicol.*, **30**, 420–433.
8. Hecht,S.S. (1998) Biochemistry, biology, and carcinogenicity of tobacco-specific N-nitrosamines. *Chem. Res. Toxicol.*, **11**, 559–603.
9. Hecht,S.S. (2008) Progress and challenges in selected areas of tobacco carcinogenesis. *Chem. Res. Toxicol.*, **21**, 160–171.
10. Guengerich,F.P., Zhao,L., Pence,M.G. and Egli,M. (2015) Structure and function of the translesion DNA polymerases and interactions with damaged DNA. *Perspect. Sci.*, **4**, 24–31.
11. Raper,A.T., Reed,A.J. and Suo,Z. (2018) Kinetic mechanism of DNA polymerases: Contributions of conformational dynamics and a third divalent metal ion. *Chem. Rev.*, **118**, 6000–6025.
12. Patra,A., Nagy,L.D., Zhang,Q.Q., Su,Y., Muller,L., Guengerich,F.P. and Egli,M. (2014) Kinetics, structure, and mechanism of 8-oxo-7,8-dihydro-2′-deoxyguanosine bypass by human DNA polymerase η. *J. Biol. Chem.*, **289**, 16867–16882.
13. Kirouac,K.N., Basu,A.K. and Ling,H. (2013) Structural mechanism of replication stalling on a bulky amino-polycyclic aromatic hydrocarbon DNA adduct by a Y-family DNA polymerase. *J. Mol. Biol.*, **425**, 4167–4176.
14. Stover,J.S., Chowdhury,G., Zang,H., Guengerich,F.P. and Rizzo,C.J. (2006) Translesion synthesis past the C8- and N2-deoxyguanosine adducts of the dietary mutagen 2-amino-3-methylimidazo[4,5-f]quinoline in the *Nar*I recognition sequence by prokaryotic DNA polymerases. *Chem. Res. Toxicol.*, **19**, 1506–1517.
15. Zhang,H., Eoff,R.L., Kozekov,I.D., Rizzo,C.J., Egli,M. and Guengerich,F.P. (2009) Versatility of Y-family *Sulfolobus solfataricus* DNA polymerase Dpo4 in translesion synthesis past bulky N2-alkylguanine adducts. *J. Biol. Chem.*, **284**, 3563–3576.
16. Eoff,R.L., Angel,K.C., Egli,M. and Guengerich,F.P. (2007) Molecular basis of selectivity of nucleoside triphosphate incorporation opposite O6-benzylguanine by *Sulfolobus solfataricus* DNA polymerase Dpo4: Steady-state and pre-steady-state kinetics and X-ray crystallography of correct and incorrect pairing. *J. Biol. Chem.*, **282**, 13573–13584.
17. Choi,J.-Y., Chowdhury,G., Zang,H., Angel,K.C., Vu,C.C., Peterson,L.A. and Guengerich,F.P. (2006) Translesion synthesis across O6-alkylguanine DNA adducts by recombinant human DNA polymerases. *J. Biol. Chem.*, **281**, 38244–38256.
18. Sherrer,S.M., Brown,J.A., Pack,L.R., Jasti,V.P., Fowler,J.D., Basu,A.K. and Suo,Z. (2009) Mechanistic studies of the bypass of a bulky single-base lesion catalyzed by a Y-family DNA polymerase. *J. Biol. Chem.*, **284**, 6379–6388.
19. Alberts,I.L., Wang,Y. and Schlick,T. (2007) DNA polymerase β catalysis: Are different mechanisms possible? *J. Am. Chem. Soc.*, **129**, 11100–11110.
20. Xu,P., Oum,L., Lee,Y.C., Geacintov,N.E. and Broyde,S. (2009) Visualizing sequence-governed nucleotide selectivities and mutagenic consequences through a replicative cycle: Processing of a bulky carcinogen N2-dG lesion in a Y-family DNA polymerase. *Biochemistry*, **48**, 4677–4690.
21. Hanwool,Y. and Arieh,W. (2017) Simulating the fidelity and the three mg mechanism of pol η and clarifying the validity of transition state theory in enzyme catalysis. *Proteins: Struct. Funct. Bioinf.*, **85**, 1446–1453.
22. Michel,A.K., Zarth,A.T., Upadhyaya,P. and Hecht,S.S. (2017) Identification of 4-(3-pyridyl)-4-oxobutyl-2′-deoxycytidine adducts formed in the reaction of DNA with 4-(acetoxymethylnitrosamino)-1-(3-pyridyl)-1-butanone: A chemically activated form of tobacco-specific carcinogens. *ACS Omega*, **2**, 1180–1190.

23. Improta,R., Santoro,F. and Blancafort,L. (2016) Quantum mechanical studies on the photophysics and the photochemistry of nucleic acids and nucleobases. *Chem. Rev.*, **116**, 3540–3593.

24. Lao,Y., Yu,N., Kassie,F., Villalta,P.W. and Hecht,S.S. (2007) Formation and accumulation of pyridyloxobutyl DNA adducts in F344 rats chronically treated with 4-(methylnitrosamino)-1-(3-pyridyl)-1-butanone and enantiomers of its metabolite, 4-(methylnitrosamino)-1-(3-pyridyl)-1-butanol. *Chem. Res. Toxicol.*, **20**, 235–245.

25. Upadhyaya,P., Lindgren,B. and Hecht,S.S. (2009) Comparative levels of O6-methylguanine, pyridyloxobutyl-, and pyridylhydroxybutyl-DNA adducts in lung and liver of rats treated chronically with the tobacco-specific carcinogen 4-(methylnitrosamino)-1-(3-pyridyl)-1-butanone (NNK). *Drug Metab. Dispos.*, **37**, 1147–1151.

26. Alexandrov,L.B., Jones,P.H., Wedge,D.C., Sale,J.E., Campbell,P.J., Nik-Zainal,S. and Stratton,M.R. (2015) Clock-like mutational processes in human somatic cells. *Nat. Genet.*, **47**, 1402–1407.

27. Gowda,A.S.P. and Spratt,T.E. (2016) DNA polymerases η and ζ combine to bypass O(2)-[4-3-pyridyl)-4-oxobutyl]thymine, a DNA adduct formed from tobacco carcinogens. *Chem. Res. Toxicol.*, **29**, 303–316.

28. Weerasooriya,S., Jasti,V.P., Bose,A., Spratt,T.E. and Basu,A.K. (2015) Roles of translesion synthesis DNA polymerases in the potent mutagenicity of tobacco-specific nitrosamine-derived O(2)-alkylthymidines in human cells. *DNA Repair*, **35**, 63–70.

29. Du,H., Leng,J., Wang,P., Li,L. and Wang,Y. (2018) Impact of tobacco-specific nitrosamine-derived DNA adducts on the efficiency and fidelity of DNA replication in human cells. *J. Biol. Chem.*, **293**, 11100–11108.

30. Hashimoto,K., Ohsawa,K.I. and Kimura,M. (2004) Mutations induced by 4-(methylnitrosamino)-1-(3-pyridyl)-1-butanone (NNK) in the *LacZ* and CII genes of Muta mouse. *Mutat. Res./Genet. Toxicol. Environ. Mutagen.*, **560**, 119–131.

31. Sandercock,L.E., Hahn,J.N., Li,L., Luchman,H.A., Giesbrecht,J.L., Peterson,L.A. and Jirik,F.R. (2008) MGMT deficiency alters the *in vivo* mutational spectrum of tissues exposed to the tobacco carcinogen 4-(methylnitrosamino)-1-(3-pyridyl)-1-butanone (NNK). *Carcinogenesis*, **29**, 866–874.

32. Jasti,V.P., Spratt,T.E. and Basu,A.K. (2011) Tobacco-specific nitrosamine-derived O2-alkylthymidines are potent mutagenic lesions in SOS-induced *Escherichia coli*. *Chem. Res. Toxicol.*, **24**, 1833–1835.

33. Stevens,D.R. and Hammes-Schiffer,S. (2018) Exploring the role of the third active site metal ion in DNA polymerase η with QM/MM free energy simulations. *J. Am. Chem. Soc.*, **140**, 8965–8969.

34. McCulloch,S.D., Kokoska,R.J., Masutani,C., Iwai,S., Hanaoka,F. and Kunkel,T.A. (2004) Preferential *cis-syn* thymine dimer bypass by DNA polymerase η occurs with biased fidelity. *Nature*, **428**, 97–100.

35. Yang,W. (2014) An overview of Y-family DNA polymerases and a case study of human DNA polymerase η. *Biochemistry*, **53**, 2793–2803.

36. Srivastava,A.K., Han,C., Zhao,R., Cui,T., Dai,Y., Mao,C., Zhao,W., Zhang,X., Yu,J. and Wang,Q.-E. (2015) Enhanced expression of DNA polymerase η contributes to cisplatin resistance of ovarian cancer stem cells. *Proc. Natl. Acad. Sci. U.S.A.*, **112**, 4411–4416.

37. Zhao,Y., Biertümpfel,C., Gregory,M.T., Hua,Y.J., Hanaoka,F. and Yang,W. (2012) Structural basis of human DNA polymerase η-mediated chemoresistance to cisplatin. *Proc. Natl. Acad. Sci. U.S.A.*, **109**, 7269–7274.

38. Malvezzi,S., Angelov,T. and Sturla,S.J. (2017) Minor groove 3-deaza-adenosine analogues: Synthesis and bypass in translesion DNA synthesis. *Chem. Eur. J.*, **23**, 1101–1109.

39. Choi,J.Y., Angel,K.C. and Guengerich,F.P. (2006) Translesion synthesis across bulky N2-alkyl guanine DNA adducts by human DNA polymerase κ. *J. Biol. Chem.*, **281**, 21062–21072.

40. Rogozin,I.B., Goncearenco,A., Lada,A.G., De,S., Yurchenko,V., Nudelman,G., Panchenko,A.R., Cooper,D.N. and Pavlov,Y.I. (2018) DNA polymerase η mutational signatures are found in a variety of different types of cancer. *Cell Cycle*, **17**, 348–355.

41. Gowda,A.S.P., Krishnegowda,G., Suo,Z., Amin,S. and Spratt,T.E. (2012) Low fidelity bypass of O2-(3-pyridyl)-4-oxobutylthymine, the most persistent bulky adduct produced by the tobacco specific nitrosamine 4-(methylnitrosamino)-1-(3-pyridyl)-1-butanone by model DNA polymerases. *Chem. Res. Toxicol.*, **25**, 1195–1202.

42. Alt,A., Lammens,K., Chiocchini,C., Lammens,A., Pieck,J.C., Kuch,D., Hopfner,K.-P. and Carell,T. (2007) Bypass of DNA lesions generated during anticancer treatment with cisplatin by DNA polymerase η. *Science*, **318**, 967–970.

43. Wilson,K.A. and Wetmore,S.D. (2017) Molecular insights into the translesion synthesis of benzyl-guanine from molecular dynamics simulations: Structural evidence of mutagenic and nonmutagenic replication. *Biochemistry*, **56**, 1841–1853.

44. Wilson,K.A. and Wetmore,S.D. (2017) Conformational flexibility of the benzyl-guanine adduct in a bypass polymerase active site permits replication: Insights from molecular dynamics simulations. *Chem. Res. Toxicol.*, **30**, 2013–2022.

45. Lior-Hoffmann,L., Ding,S., Geacintov,N.E., Zhang,Y. and Broyde,S. (2014) Structural and dynamic characterization of polymerase κ's minor groove lesion processing reveals how adduct topology impacts fidelity. *Biochemistry*, **53**, 5683–5691.

46. Wang,L., Wu,M., Yan,S.F., Patel,D.J., Geacintov,N.E. and Broyde,S. (2005) Accommodation of a 1s-(−)-benzo[c]phenanthrenyl-N6-dA adduct in the Y-family Dpo4 DNA polymerase active site: Structural insights through molecular dynamics simulations. *Chem. Res. Toxicol.*, **18**, 441–456.

47. Perera,L., Freudenthal,B.D., Beard,W.A., Shock,D.D., Pedersen,L.G. and Wilson,S.H. (2015) Requirement for transient metal ions revealed through computational analysis for DNA polymerase going in reverse. *Proc. Natl. Acad. Sci. U.S.A.*, **112**, E5228–E5236.

48. Lin,P., Batra,V.K., Pedersen,L.C., Beard,W.A., Wilson,S.H. and Pedersen,L.G. (2008) Incorrect nucleotide insertion at the active site of a G:A mismatch catalyzed by DNA polymerase β. *Proc. Natl. Acad. Sci. U.S.A.*, **105**, 5670–5674.

49. Kropp,H.M., Dürr,S.L., Peter,C., Diederichs,K. and Marx,A. (2018) Snapshots of a modified nucleotide moving through the confines of a DNA polymerase. *Proc. Natl. Acad. Sci. U.S.A.*, **115**, 9992–9997.

50. Liyanage,P.S., Walker,A.R., Brenlla,A., Cisneros,G.A., Romano,L.J. and Rueda,D. (2017) Bulky lesion bypass requires Dpo4 binding in distinct conformations. *Scientific Rep.*, **7**, 17383.

51. Vaisman,A. and Woodgate,R. (2017) Translesion DNA polymerases in eukaryotes: What makes them tick? *Crit. Rev. Biochem. Mol. Biol.*, **52**, 274–303.

52. Norman,D., Abuaf,P., Hingerty,B.E., Live,D., Grunberger,D., Broyde,S. and Patel,D.J. (1989) NMR and computational characterization of the N-(deoxyguanosin-8-yl) aminofluorene adduct [(AF) G] opposite adenosine in DNA:(AF) G [*syn*]:A [*anti*] pair formation and its pH dependence. *Biochemistry*, **28**, 7462–7476.

53. Gu,Z., Gorin,A., Hingerty,B.E., Broyde,S. and Patel,D.J. (1999) Solution structures of aminofluorene [AF]-stacked conformers of the syn [AF]−C8-dG adduct positioned opposite dC or dA at a template-primer junction. *Biochemistry*, **38**, 10855–10870.

54. Hu,L., Li,Z., Cheng,J., Rao,Q., Gong,W., Liu,M., Shi,Y.G., Zhu,J., Wang,P. and Xu,Y. (2013) Crystal structure of TET2-DNA complex: Insight into TET-mediated 5mC oxidation. *Cell*, **155**, 1545–1555.

55. Imamura,K., Averill,A., Wallace,S.S. and Doublié,S. (2012) Structural characterization of viral ortholog of human DNA glycosylase Neil1 bound to thymine glycol or 5-hydroxyuracil-containing DNA. *J. Biol. Chem.*, **287**, 4288–4298.

56. Sokoloski,J.E., Godfrey,S.A., Dombrowski,S.E. and Bevilacqua,P.C. (2011) Prevalence of *syn* nucleobases in the active sites of functional RNAs. *RNA*, **17**, 1775–1787.

57. Brautigam,C.A. and Steitz,T.A. (1998) Structural and functional insights provided by crystal structures of DNA polymerases and their substrate complexes. *Curr. Opin. Struct. Biol.*, **8**, 54–63.

58. Wang,Y. and Schlick,T. (2008) Quantum mechanics/molecular mechanics investigation of the chemical reaction in Dpo4 reveals water-dependent pathways and requirements for active site reorganization. *J. Am. Chem. Soc.*, **130**, 13240–13250.

59. Wang,L., Yu,X., Hu,P., Broyde,S. and Zhang,Y. (2007) A water-mediated and substrate-assisted catalytic mechanism for *Sulfolobus solfataricus* DNA polymerase IV. *J. Am. Chem. Soc.*, **129**, 4731–4737.

60. Patra,A., Zhang,Q., Lei,L., Su,Y., Egli,M. and Guengerich,F.P. (2015) Structural and kinetic analysis of nucleoside triphosphate incorporation opposite an abasic site by human translesion DNA polymerase η. *J. Biol. Chem.*, **290**, 8028–8038.